Applied Catalysis B: Environmental 203 (2017) 108–115

Contents lists available at ScienceDirect

Applied Catalysis B: Environmental

journal homepage: www.elsevier.com/locate/apcatb

Ultrathin graphitic C_3N_4 nanosheet as a promising visible-light-activated support for boosting photoelectrocatalytic methanol oxidation

Mingshan Zhu [a,c,*], Chunyang Zhai [a], Mingjuan Sun [a], Yufang Hu [a], Bo Yan [b], Yukou Du [a,b,*]

[a] School of Materials Science and Chemical Engineering, Ningbo University, Ningbo 315211, PR China
[b] College of Chemistry, Chemical Engineering and Materials Science, Soochow University, Suzhou 215123, PR China
[c] The Institute of Scientific and Industrial Research, Osaka University, Osaka 567-0047, Japan

ARTICLE INFO

Article history:
Received 12 August 2016
Received in revised form
26 September 2016
Accepted 8 October 2016
Available online 11 October 2016

Keywords:
Carbon nitride
Photo-responsive electrode
Visible light
Photoelectrocatalysis
Methanol oxidation

ABSTRACT

In this paper, ultrathin two dimensional (2D) g-C_3N_4 nanosheet worked as support for the deposition of ultrasmall Pt nanoclusters. The average size of Pt nanocluster is about 3.2 nm. Firstly, the as-prepared Pt/g-C_3N_4 modified electrode exhibited enhanced electrocatalytic ability in methanol oxidation reaction (MOR) compared to bare Pt nanoparticles. Moreover, when this electrode was upon visible light irradiation, higher performance of MOR was clearly observed compared to the traditional ambient electrocatalytic oxidation. This is owing to the synergistic effects of photocatalytic and electrocatalytic MOR together with the efficient interfacial charger transfer in Pt/g-C_3N_4. These results show that 2D ultrathin g-C_3N_4 nanosheets can be used as promising photoactived support in the fields of solar and chemical energy conversion and also provide more insights into developing novel visible light photo-responsive electrode in direct methanol fuel cell.

1. Introduction

One of the promising technologies for future alternative energy sources is the conversion of solar and chemical energy into electrical energy by using photoelectrocatalysis [1–4]. Since Kamat's group first reported the enhanced methanol oxidation reaction (MOR) fuel cell performance by using photoactivated Pt-Ru/TiO_2 electrode under UV light irradiation [5], the photo-responsive metal/semiconductor hybrids as anode catalysts received more and more attractions for improving the activity and stability of fuel cell reaction [4–15]. Up to date, most of semiconductor materials which had been used for MOR are consisted of metal oxide, such as TiO_2. However, the large band gap (3.2 eV) of TiO_2 might limit the broad application because of its only shows activity under UV irradiation (<5% of the solar energy) [16]. Moreover, owing to no active sites on the conventional semiconductor skeleton, the poor hybridization between metal and semiconductor supports also may hinder the improvement of photoelectrocatalytic performance. The greatest challenge in this field is to develop novel materials with the desired optical properties and structure that will replace conventional materials that are currently used.

Currently, graphite-like carbon nitride (g-C_3N_4), as a polymeric semiconductor, has considered to be a promising visible light active candidate for water splitting; fuel cells, degradation of pollutants and organic photosynthesis [17–20]. This is because its possesses high thermal and chemical stability, low cost of mass production and an appealing electronic structure with appropriate band gap which suitable for a variety of relevant chemical reactions. More importantly, carbon nitride matrix can provide coordination to various metal due to the nitrogen rich polymeric semiconductors structurally (C/N = 0.75, a heterocyclic macrocycle structure with N—C—N—bonding pattern) [19–25], which acts as Lewis basic sites (various amino groups), as shown in Scheme S1. This unique feature endows with g-C_3N_4 abundant reactive sites for the construction of metal/g-C_3N_4 hybrids, in which the g-C_3N_4 might not only work as template but also as a photoactive support for anchoring metal nanostructures in the improvement of the photoelectrocatalytic performance.

Herein, for the first time, using ultrathin g-C_3N_4 nanosheet as a photoactivated support for the decoration of Pt nanoclusters, great improvement of photoelectrocatalytic performance for methanol oxidation reaction (MOR) was achieved under visible

* Corresponding authors at: School of Materials Science and Chemical Engineering, Ningbo University, Ningbo 315211, PR China.
E-mail addresses: mingshanzhu@yahoo.com (M. Zhu), duyk@suda.edu.cn (Y. Du).

http://dx.doi.org/10.1016/j.apcatb.2016.10.012
0926-3373/

light irradiation. Firstly, well dispersions of Pt nanoclusters with a diameter of 3.2 nm were deposited on the surface of ultrathin g-C_3N_4 nanosheets. Furthermore, these Pt/g-C_3N_4 composites display highly electrocatalytic performance towards MOR performance under visible light irradiation. Compared to traditional ambient reaction, the as-prepared Pt/g-C_3N_4 composite displayed 3.3 and 1.9 times enhanced catalytic activity of MOR under visible light illumination in alkaline and acid medium, respectively. The outstanding photoelectrocatalytic activities suggest that the 2D g-C_3N_4 can be served as an ideal photo-activated support for the commercialization of direct methanol fuel cells in future. Along with the physical understanding of our materials, this research will also encompass significant work in materials science towards an innovative design, synthesis and fabrication of a new generation for energy conversion photoelectrocatalysts.

2. Experimental section

2.1. Materials and characterization

Urea [$CO(NH_2)_2$], chloroplatinic acid hexahydrate ($H_2PtCl_6{\cdot}6H_2O$), potassium hydroxide (KOH), sulphuric acid (H_2SO_4), methanol (CH_3OH) and ethanol (CH_3CH_2OH) were purchased from Sinopharm Chemical Reagent Co., Ltd. without further purification before use. High-purity deionized water was used during the experiments.

Transmission electron microscopy (TEM) was measured on TecnaiG220 (FEI America) operating at 200 kV. AFM image was recorded using a nanoscale hybrid microscope (Keyence VN-8010). The sample was prepared by spraying a diluted suspension of sample on a freshly cleaved mica surface and then dried in air. A PANalytical X' Pert PRO MRD system with Cu Ka radiation was used to obtain X-ray diffraction (XRD) patterns of the samples. The ESCALab220i-XL electron spectrometer was employed for X-ray photoelectron spectroscopy (XPS) testing. The adventitious carbon (the C 1s line at 284.8 eV) was used as reference to binding energies. UV–vis diffuse reflectance spectra were recorded on the UV–vis–NIR Shimadzu UV3150 spectrophotometer. Photoluminescence (PL) spectra were measured at room temperature on Edinburgh FLS920 fluorospectrophotometer. The excitation wavelength was 405 nm.

2.2. Synthesis of ultrathin g-C_3N_4 and Pt-C_3N_4 nanocomposites and corresponding modified electrodes

The g-C_3N_4 nanosheets were synthesized by heating urea in the semiclosed system to prevent sublimation of urea [26]. Typically, 10 g of urea powder was firstly dissolved into 15 mL water and then adjust the pH to 4–5 by using HCl. After that, the urea solution was dried at 60 °C for 12 h and then put into a crucible with a lid. The precursor was heated to 550 °C in muffle furnace at a heating rate of 10 °C min^{-1}, and maintained at 550 °C for 2 h, resulting in ultrathin g-C_3N_4 nanosheets.

The Pt/g-C_3N_4 nanocomposite was synthesized by a simple reflux method, with ethanol as the reducing agent [27]. The preparation process follows: 30 mg of g-C_3N_4 and 0.45 mL H_2PtCl_6 (3.8×10^{-2} mol L^{-1}) were dispersed in 50 mL ethanol-water mixtures ($V_{ethanol}$:V_{water} = 1:1) with sonication for 2 h to ensure the H_2PtCl_6 was dispersed in the g-C_3N_4 suspension. Then, the mixture solution was stirring at 80 °C for 2 h. After that, the powders were collected by centrifugation and washed with water thoroughly, and then dried in an oven at 40 °C for 6 h to obtain Pt/g-C_3N_4 nanocomposite. The weight ratio of g-C_3N_4 to Pt was 10:1.

The modified electrodes were prepared as follow: 1 mg samples and 10 μL Nafion solutions (5 wt.%) were added into a water/ethanol mixture ($V_{ethanol}$:V_{water} = 1:1; 1 mL) under ultrasonication for 30 min to form a homogeneous ink. Then, 5 μL of the well dispersed catalyst ink (containing 1.1 μg of Pt catalyst) was dropped onto the glassy carbon electrode (GCE, 3 mm in diameter) and dried in air at room temperature.

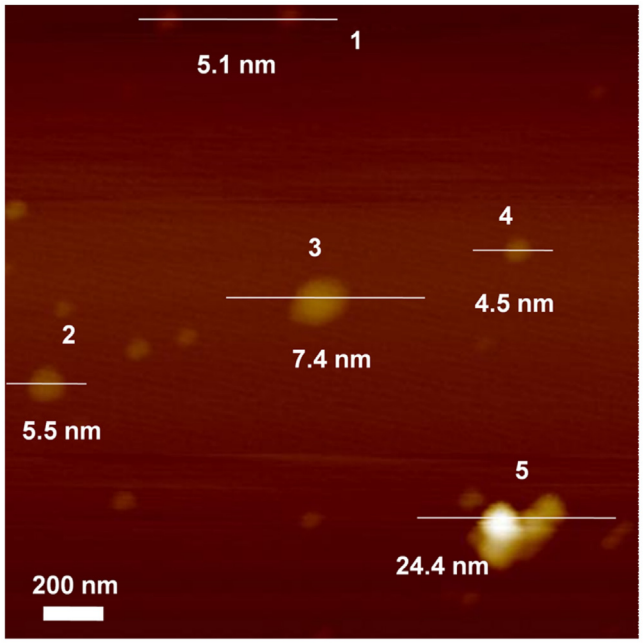

Fig. 1. AFM image of as-prepared g-C_3N_4 nanosheets.

2.3. Electro- and photo-catalytic performances

The electrochemical measurements were carried out in quartz beaker by using an electrochemical workstation (CHI 660E) in a three-electrode system devised of a modified GC, a saturated calomel electrode (SCE) and a Pt wire as working, counter and reference electrodes, respectively. The electrochemical activity of MOR was measured by CV measurements at a scan rate of 50 mV s^{-1} from −1.0 to 0.2 V in the mixture of 1.0 M methanol + 1.0 M KOH or 1.0 M H_2SO_4. The electrochemical active surface area (ECSA) study and cyclic voltammetry (CV) measurements were performed in 1.0 M KOH solution at a scan rate of 50 mV s^{-1} from −1.0 to 0.2 V (SCE). Chronoamperometry (CA) and photocurrent responses of the g-C_3N_4-based modified electrodes under dark or visible light irradiation were measured at −0.3 V at a scan rate of 50 mV s^{-1}. 2.5 mM $K_3[Fe(CN)_6/K_4[Fe(CN)_6]$ (1:1) mixture as a redox probe in the aqueous solution of KCl (0.1 M) at 0.3 V was measured for electrochemical impedance spectroscopy (EIS) measurements. Different potentials of EIS were carried out by using 1.0 M CH_3OH + 1.0 M KOH solution under an AC voltage amplitude of 5.0 mV over the frequency range between 0.1 and 10^5 Hz. All of the measurements were carried out at room temperature.

The working electrode was irradiated through a xenon lamp (150 W), which equipped with UV cut–off filter (>400 nm), for visible light photo-electrochemical measurements.

3. Results and discussion

Experimentally, the g-C_3N_4 nanosheets were easily obtained by a thermal polymerization method. To explore the thickness of as-synthesized g-C_3N_4 nanosheets, the samples were investigated by means of AFM. As shown in Fig. 1, the thickness of g-C_3N_4 nanosheets ranging from 4.5 to 24.4 nm was observed (the height profiles for different nanosheets were shown in Fig. S1), suggest-

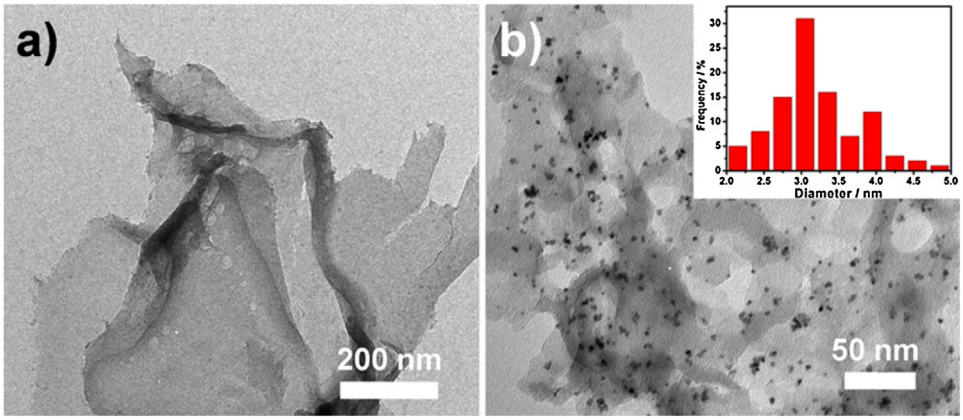

Fig. 2. TEM images of pure ultrathin g-C_3N_4 nanosheets (a) and Pt/g-C_3N_4 nanocomposites (b). The insert of Fig. 2b is the size distribution of Pt nanoparticles in Pt/g-C_3N_4 nanocomposites.

ing ultrathin 2D morphology of the as-synthesized g-C_3N_4. Fig. 2a shows the TEM image of g-C_3N_4 nanosheets. It's also easily to see the ultrathin sheet-like structures of as-prepared sample. Using this 2D material as support, well dispersions of Pt nanoclusters were deposited on the surface of g-C_3N_4 nanosheets, as shown in Fig. 2b. The average diameter of Pt on the surface of g-C_3N_4 nanosheets is *ca.* 3.2 nm. Usually, the 2D nanosheets such as graphene, MoS_2, etc., could be acted as a promising substrate for the growth of noble metal clusters, which will result in a smaller size of the noble metal clusters [28]. The bare Pt nanoparticles (NPs) were synthesized by similar method without any supports or surfactants for comparison (Fig. S2). The average size of these Pt NPs was *ca.* 50 nm, which is much larger than the Pt on the surface of g-C_3N_4 nanosheets, suggesting that the ultrathin g-C_3N_4 nanosheets can be worked as superior supports for preparing ultrasmall size of noble metal nanoparticles.

To confirm the component and the crystal structure of as-synthesized samples, XRD patterns and XPS spectra of g-C_3N_4 nanosheets and Pt/g-C_3N_4 nanocomposites were measured. As shown in Fig. 3A, the primary peak for both samples appears at 27.4° corresponding to the diffraction from (002) plane of g-C_3N_4 nanosheets [22]. Beside this peak, the diffraction peaks at 39.9°, 46.4°, 67.7°, and 81.6° were observed in the Pt/g-C_3N_4 nanocomposites, which can be assigned to the diffraction of the (111), (200), (220) and (311) crystal planes of Pt [27]. This result suggests the formation of Pt NPs in Pt/g-C_3N_4 nanocomposites.

The XPS spectra of C 1s, N 1s, and Pt 4f of the g-C_3N_4 and Pt/g-C_3N_4 nanosheets are plotted in Fig. 3B–D. Firstly, for C 1s spectra, beside the standard C 1s line at 284.8 eV from adventitious carbon, a binding energy of 288.2 eV, corresponding to a C—N—C coordination was observed in the both samples, shown in Fig. 3B [24]. Furthermore, Fig. 3C shows three peaks at 398.7, 400.2, and 401.4 eV. The former peak can be assigned to C—N<C—>C groups [24], the peak at 400.2 eV can be attributed to tertiary nitrogen N-C3 groups [24,25], and the peak at 401.4 eV was corresponding to the amino functions carrying hydrogen (C—N—H) [24,25]. Moreover, when the Pt nanoclusters were introduced into the g-C_3N_4 structures, the binding energy of N 1s slightly shift to higher binding energy (~398.8 eV) in the XPS spectra (Fig. 3C). This small shift toward higher energy confirms that the g-C_3N_4 in the nanocomposites of Pt/g-C_3N_4 works as an electron donor during the photoreaction process [16,29], leading to the facilitated charged separation. The Pt 4f shows (Fig. 3D) doublet peaks originating from the spin orbital splitting of the $4f_{7/2}$ and $4f_{5/2}$ states, in which at 72.2 and 75.5 eV, respectively. This result agrees well with the values for Pt [13], suggesting that the Pt can be detected in the Pt/g-C_3N_4 nanosheets.

To analyze the optical properties of the as-prepared g-C_3N_4 and Pt/g-C_3N_4 samples, the UV–vis diffuse reflectance spectra of both samples were measured, as shown in Fig. 3E. The g-C_3N_4 nanosheets showed an absorption edge at *ca.* 458 nm, revealing the semiconductor g-C_3N_4 with band gap of 2.7 eV [20]. When the Pt nanoclusters were deposited on the surface of g-C_3N_4 nanosheets, a tail absorption edge was observed, likely because the presence of Pt NPs [13]. These distinct absorptions in the visible range suggest that the as-prepared samples have potential advantages to photoelectrocatalytic MOR by utilizing visible light.

The photoelectric properties of the as-prepared Pt/g-C_3N_4 nanosheets modified electrodes were evaluated by using the photocurrent response, photoluminescence (PL), cyclic voltammograms (CVs) and electrochemical impedance spectrum (EIS), as shown in Fig. 4. Fig. 4A shows photocurrent–time (*I–t*) curve on the Pt/g-C_3N_4 electrode. When the electrode was upon visible light illumination, a responsive photocurrent with intensity of *ca.* 60 $\mu A\,cm^{-2}$ was observed. The photocurrent response also was repeatable during on/off cycles upon light illumination. However, the control experiment of bare Pt and g-C_3N_4 showed no photocurrent response (result not shown) and 3 $\mu A\,cm^{-2}$ (insert of Fig. 4A), respectively.

The effective of photoresponse of the Pt/g-C_3N_4 electrode was attributed to the interfacial charge transfers of photoexcited g-C_3N_4 nanosheets and Pt nanoclusters. To investigate this interfacial charge transfer between g-C_3N_4 nanosheets and Pt nanoclusters, the PL emission spectra of pure g-C_3N_4 nanosheets and Pt/g-C_3N_4 nanocomposites were investigated. Fig. 4B shows typical PL emission spectrum of g-C_3N_4, which a broad peak at *ca.* 467 nm was observed when samples were excited at 405 nm. However, when Pt NPs were deposited on the surface of g-C_3N_4 nanosheets, evidently PL emission quenching with *ca.* 80% was observed. This result clearly indicates that the photoexcited electron from g-C_3N_4 nanosheets can be trapped by Pt efficiently [30].

In addition, $K_3[Fe(CN)_6]/K_4[Fe(CN)_6]$ (1:1) mixture was used as a redox probe to investigate the effective charge transfer during the photoreactions of the Pt/g-C_3N_4 nanocomposites modifed electrode. Fig. 4C shows the CV responses of reversible redox couple of $Fe(CN)_6^{4-}/Fe(CN)_6^{3-}$ on Pt/g-C_3N_4 electrode under both dark and visible light illumination. When the as-prepared electrode was under visible light irradiation, the peaks of redox potential were shifted to lower potentials compared to the same electrode without light irradiation. Moreover, the redox peak current was also improved upon light irradiation. In addition, the EIS data were analyzed by using Nyquist plots in the range of 0.1 Hz–100 kHz with and without visible light irradiation. Fig. 4D shows that the diameter of the semicircle arc of the Pt/g-C_3N_4 modified elec-

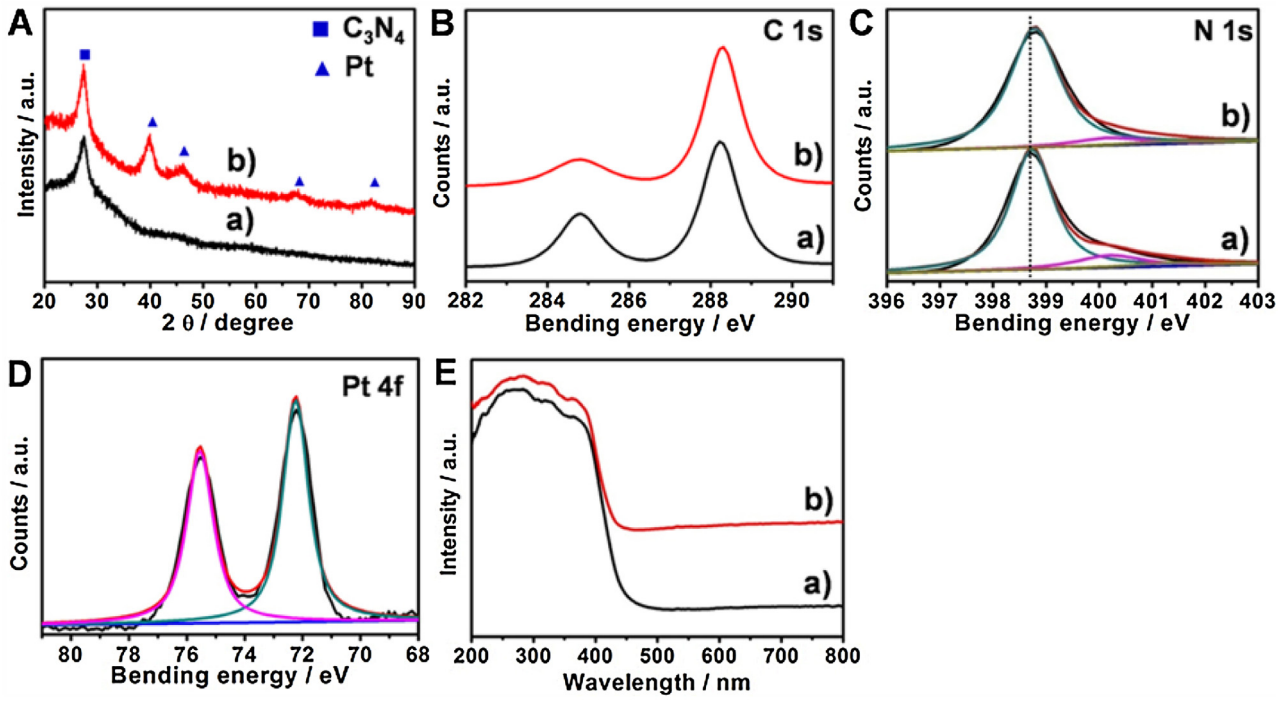

Fig. 3. XRD patterns (A), XPS spectra of C 1s (B), N 1s (C) and UV–vis spectra (E) of ultrathin g-C_3N_4 nanosheets (a) and Pt/g-C_3N_4 nanocomposites (b). XPS spectrum of Pt 4f (D) of Pt/g-C_3N_4 nanocomposites.

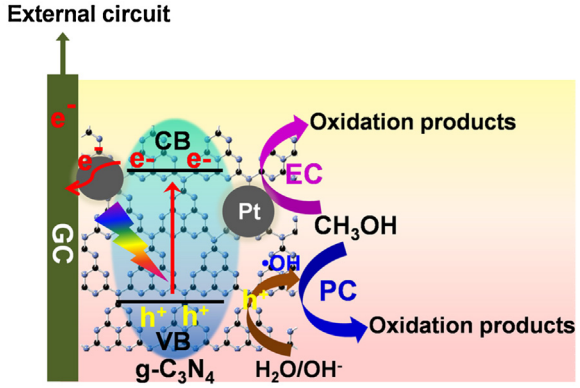

Scheme 1. Schematic illustration for the synergistic electrocatalytic (EC) and photocatalytic (PC) MOR by using the Pt/g-C_3N_4 modified electrode under visible-light irradiation.

trode in $K_3[Fe(CN)_6]/K_4[Fe(CN)_6]$ mixture upon light irradiation was smaller than that under dark condition. We also investigated the corresponding EIS of Pt/g-C_3N_4 electrode under dark and visible light irradiation in a 1.0 M CH_3OH + 1.0 M KOH solution. Fig. S3 shows similar results compared to above results. These results further indicate a decrease internal resistancy and significant improvement of interfacial electron transfer in the photoilluminated Pt/g-C_3N_4 electrode [13,31].

To demonstrate the superior photoelectrocatalytic performance of Pt/g-C_3N_4 modified electrode, the electrochemically active surface areas (ECSAs) of pure Pt NPs and Pt/g-C_3N_4 nanosheets modified electrodes need to be firstly measured. The ECSAs were derived by calculation of the H_2 desorption area according to Eq. (1) [32]

$$\mathrm{ECSA} = \frac{Q_H}{0.21 \times [\mathrm{Pt}]} \quad (1)$$

where Q_H represents the charge for hydrogen adsorption/desorption (mC cm^{-2}), *[Pt]* represents the Pt loading (mg cm^{-2}) in the electrode, and 0.21 mC cm^{-2} represents the maximum surface charge transferred to Pt during adsorption of a monolayer of H. The Q_H were derived by calculation the charger for hydrogen adsorption/desorption area according to Eq. (2):

$$Q_H = \frac{Q_{H_{ads}} + Q_{H_{des}}}{2} \quad (2)$$

the $Q_{H_{ads}}$ and $Q_{H_{des}}$ represent the charge for H-adsorption and H-desorption peak area, respectively [33]. As shown in Fig. 5A, the CVs were performed from −0.1 V to 0.2 V in a N_2-saturated 1.0 M KOH solution. The cathodic and anodic peaks appearing between −1.0 and −0.6 V versus SCE originate from H-adsorption and H-desorption, respectively [34]. The integrated area of the H_2 absorption and desorption peaks for Pt/g-C_3N_4 nanocomposites is evidently larger than that of bare Pt NPs, in which the ECSAs of Pt/g-C_3N_4 nanosheets and pure Pt NPs are 12.87 and 10.58 cm^2 mg^{-1}, respectively. The small size of Pt nanoclusters on the surface of g-C_3N_4 nanosheets attributes to larger ECSAs compared to the aggregated Pt NPs. The larger ECSA means that the Pt/g-C_3N_4 has more active sites in the electrocatalytic process. This result suggests that g-C_3N_4 can be worked as promising support of Pt electrocatalysts, which might have great potential in anodic fuel cell reactions.

The linear sweep voltammetric (LSV) behaviors of pure Pt NPs and Pt/g-C_3N_4 modified electrodes under dark and light illumination in a 1.0 M CH_3OH + 1.0 M KOH solution were also studied, as shown in Fig. 5B. The onset potential on the Pt/g-C_3N_4 electrode with light illumination was negatively shift compared to that without light irradiation. Furthermore, at a given potential of −0.3 V, the current density of Pt/g-C_3N_4 electrode was 132 mA mg^{-1} under light illumination, which is *ca.* 2.4 and 3.1 times higher than that of Pt/g-C_3N_4 without light irradiation (56.0 mA mg^{-1}) and of Pt NPs electrode (42.3 mA mg^{-1}), respectively. The negative shift onset potential and improved current density of Pt/g-C_3N_4 under light illumination were attributed to that the supporter g-C_3N_4 not only

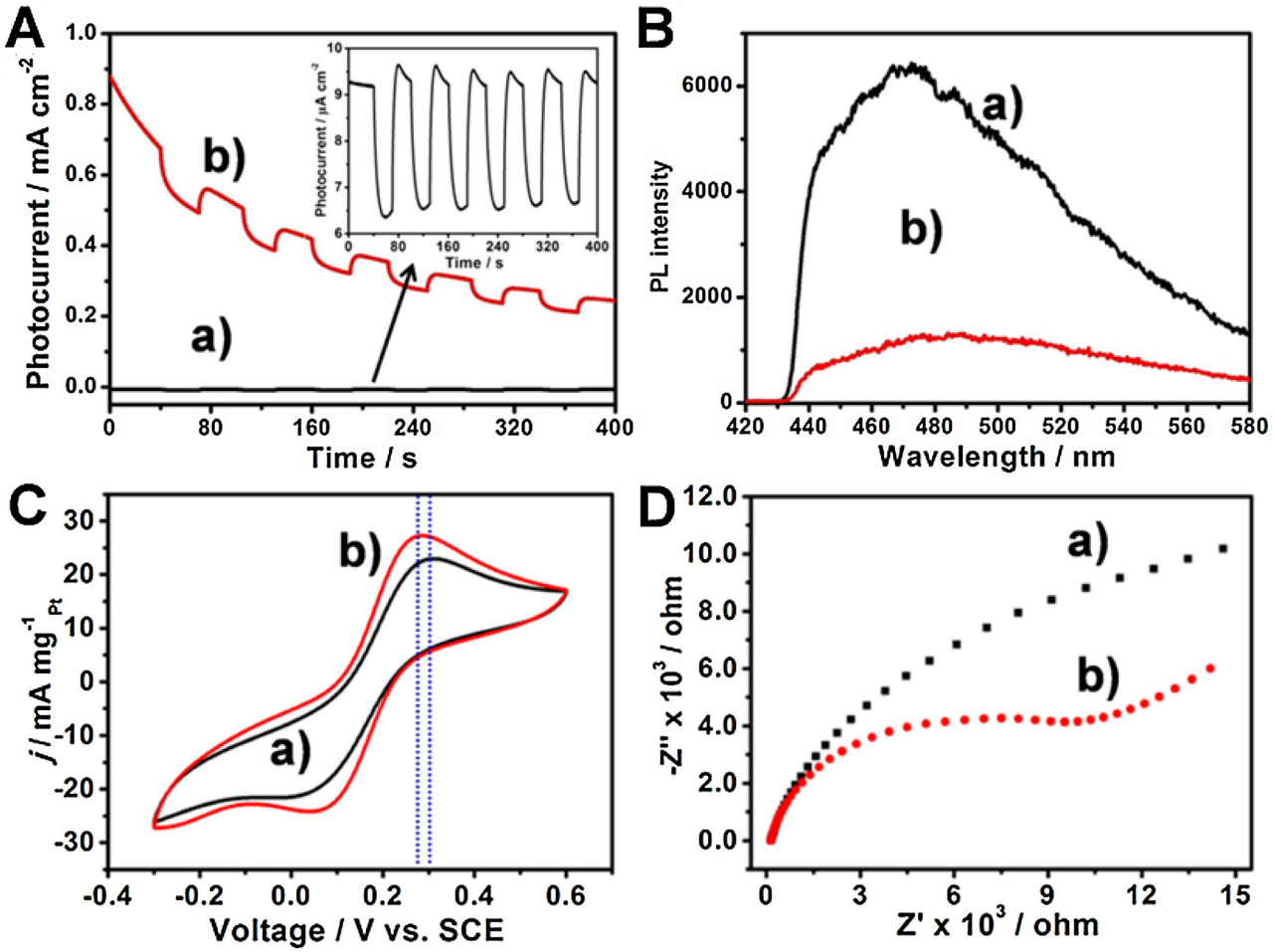

Fig. 4. Photocurrent responses (A) and PL emission spectra (B) of the ultrathin g-C_3N_4 nanosheets (a) and Pt/g-C_3N_4 nanocomposites (b). The photocurrent responses of the working electrode were in 1.0 M CH_3OH and 1.0 M KOH solution at a potential of −0.3 V under visible light illumination. The illumination from a Xe lamp was interrupted every 30 s. The PL excitation wavelength: 405 nm. CVs (C) and EIS spectra of (D) of the Pt/g-C_3N_4 electrode in a 2.5 mM $K_3[Fe(CN)_6]/K_4[Fe(CN)_6]$ and 0.1 M KCl solution at a potential of 0.3 V (a) without and (b) with visible-light irradiation.

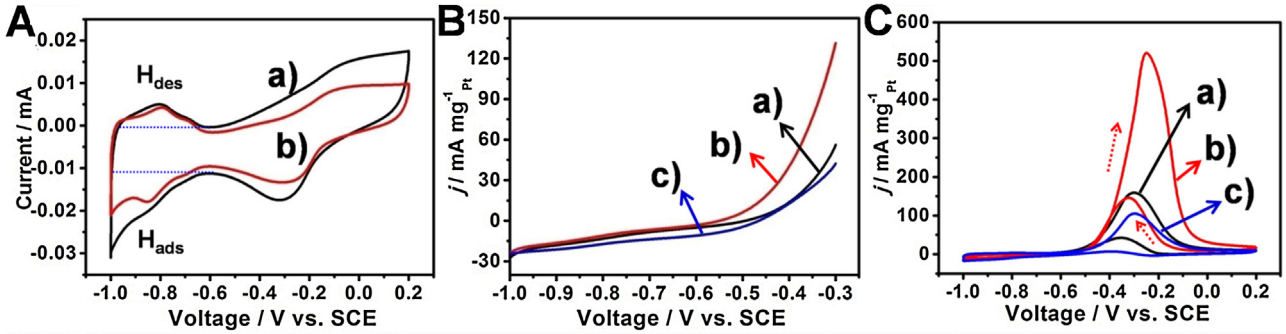

Fig. 5. A: CVs of the Pt/g-C_3N_4 (a) and pure Pt NPs (b) modified electrode in 1.0 M KOH solution at a scan rate of 50 mV s^{-1}. Linear sweep voltammetry (B) and the 170th CVs (C) of the Pt/g-C_3N_4 under dark (a) and visible light illumination (b), and pure Pt NPs (c) in 1.0 M CH_3OH + 1.0 M KOH solution at a scan rate of 50 mV s^{-1}.

increased the Pt well-dispersion but also acted as photocatalyst to generate photogenerated charges.

The photoelectrocatalytic activities of the as–prepared Pt/g-C_3N_4 nanocomposites modified electrode were evaluated by MOR. Fig. 5C shows the CVs of pure Pt NPs and Pt/g-C_3N_4 nanosheets modified electrode under dark and visible light irradiation in a 1.0 M CH_3OH + 1.0 M KOH solution. The curves show typical profiles for the electrooxidation of methanol between −1.0 V and 0.2 V with two strong oxidation peaks. It is observed that the forward peak current intensity of Pt/g-C_3N_4 nanosheets can be reached to 158.9 mA mg^{-1}, which is higher than that of pure Pt NPs modified electrode (104.8 mA mg^{-1}). For control experiment, the bare GC and g-C_3N_4 electrodes showed negligible electrocatalytic activities toward methanol oxidation, as shown in Fig. S4. The enhancement of the electrocatalytic activity of MOR for Pt/g-C_3N_4 was attributed to that the 2D property of ultrathin g-C_3N_4 nanosheets can improve the dispersion of active Pt NPs and the adsorption of target molecules on the support surface.

More interesting, when the Pt/g-C_3N_4 nanocomposite modified electrode was under visible light irradiation, the current

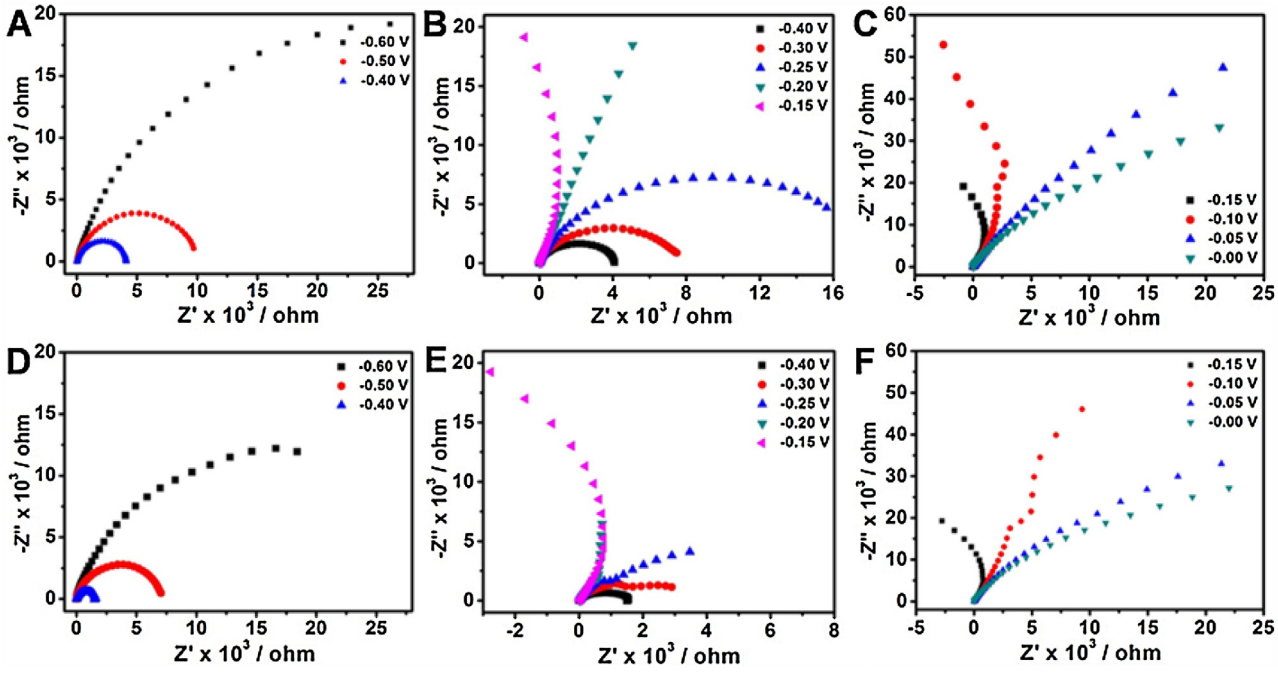

Fig. 6. Nyquist plots of the Pt-C_3N_4 electrode in 1.0 M CH_3OH + 1.0 M KOH solution at electrode potentials from −0.6 V to 0 V without (A–C) and with (D–F) visible light illumination.

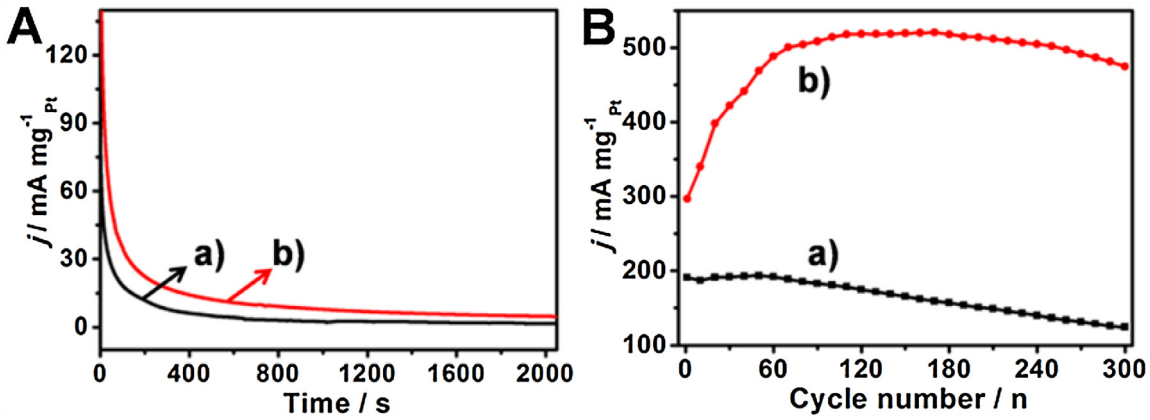

Fig. 7. Chronoamperometric curves (A) and the peak current of MOR in the forward scan *vs.* the CV cycle number (B) on Pt/g-C_3N_4 modified electrode under dark (a) and visible light illumination (b).

intensity can be great improved and reached to 520.4 mA mg^{-1}. Compared to the traditional electrocatalytic performance of MOR by using bare Pt NPs and Pt/g-C_3N_4 nanosheets modified electrode, this photoilluminated Pt/g-C_3N_4 electrode displayed 5.0 and 3.3 times, respectively. The similar enhanced catalytic performances were observed when the as-prepared electrode was upon visible light irradiation with >420 nm filter (Fig. S5). Moreover, the Pt/g-C_3N_4 electrode was also evaluated in the acid medium with 1.0 M CH_3OH + 1.0 M H_2SO_4 under dark and visible light irradiation. As shown in Fig. S6, the similar phenomenon was observed. The catalytic performance of MOR can be improved easily in the presence of light illuminated. Since Kamat's group first reported on this phenomenon by using UV light enhanced MOR performance on photoactivated a Pt-Ru/TiO_2 electrode, the synergistic effects of electro- and photo- catalytic oxidation of methanol were proposed [4–15].

The proposed mechanism of the above enhanced MOR performance was illustrated, as shown in Scheme 1. Firstly, for traditional electrocatalytic MOR process, the Pt NPs were served as active sites and the methanol molecules would be electro-oxidized to CO_2 on the surface of Pt. The introduced ultrathin g-C_3N_4 as a support will not only prevent the aggregation of Pt during the synthesis process, resulting in a small size of Pt nanoparticles, but also in favor of adsorption of target molecules owing to 2D structures. On the other hand, when the Pt/g-C_3N_4 electrode was upon visible light (>400 nm) irradiation, the g-C_3N_4 can be excited and generated electrons (e_{CB}^-) in the conduction band (CB) and holes (h_{VB}^+) in the valence band (VB) [17–20]. Therein, the holes have oxidative ability and can react with surface adsorbed OH^-/H_2O to form strong oxidative hydroxyl radicals (•OHs) [6–9]. The adsorbed methanol molecules on the surface of catalysts can be also oxidized upon these •OHs, leading to a photocatalytic MOR process [6–9]. Usually, these electron-hole pairs will quickly recombine and only a fraction of holes can be used. In the as-prepared Pt/g-C_3N_4 nanocomposites, the effective interfacial charge transfers between photoexcited g-C_3N_4 nanosheets and Pt nanoclusters were demonstrated in the above photocurrent response, PL, CVs and EIS (Fig. 4). The photoex-

cited electrons will transfer to Pt firstly and then flow to circuit under external electric field, thus preventing the charges recombination.

To give further evidence to support the above suggested synergistic electro- and photo- catalysis of MOR mechanism, the EIS in different potential range of as-prepared Pt/g-C_3N_4 nanosheets modified electrode with and without light irradiation were investigated. As shown in Fig. 6A, from −0.60 V to −0.40 V, the diameters of the impedance arcs (DIA) decreases greatly with increasing potential under dark condition. This result means that at lower potential, more active sites were available for MOR due to the oxidation removal of CO intermediate species, which generate from methanol dehydrogenation [35,36]. When the potential continue increased (from −0.4 V to −0.20 V, Fig. 6B), the DIA began to increase due to the poisoning and oxidation of catalyst at relative higher potentials. However, the arc suddenly reversed to the second quadrant at −0.15 V. The negative behavior is owing to the oxidation removal of CO from the catalyst surface and the recovery of catalytic active sites. At more positive potentials from 0 V to −0.15 V (Fig. 6C), the arcs changed to normal positive behavior gradually with a large DIA. This is because of the CO intermediate species were absent while the Pt might be covered by Pt oxides, inhibiting the oxidation of methanol [35].

Compared to the traditional electrocatalytic process, when the Pt/g-C_3N_4 electrode was upon light illumination, the smaller DIAs were observed compared to that under same potential (Fig. 6D). This result indicates that the charge-transfer resistance (R_{ct}) of MOR during photoassisted process is smaller. For continuous increase the applied potential, the arc reversed to the second quadrant at −0.20 V (Fig. 6E), which was lower than that of Pt/g-C_3N_4 electrode without light illumination (−0.15 V). The more negative onset potential of negative impedance compared with dark condition suggested that the oxidation removal of CO species on surface of Pt/g-C_3N_4 electrode was easily [13]. With the similar phenomenon, from 0 V to −0.15 V (Fig. 6F), the arcs turned to normal positive behavior gradually with a large DIA, while the tendency of arc turned back to the first quadrant at −0.10 V was more obviously. Moreover, as the Nyquist plots shown, the DIAs were smaller in the whole potential range than corresponding of potential on Pt/g-C_3N_4 electrode without light illumination. These smaller DIAs mean smaller R_{ct}, which is owing to the effective interfacial charge transfer on Pt/g-C_3N_4 electrode upon light illumination, following higher photoelectrocatalytic MOR performance.

The stability of catalyst is an important parameter to evaluate electrocatalyst in fuel cells. As shown in Fig. 7, chronoamperometric curve and scan cycling experiments were used to determine the stability of the as-prepared Pt/g-C_3N_4 electrode. The current densities changes in 2000 s for Pt/g-C_3N_4 electrode with and without visible light illumination were shown in Fig. 7A. The electrode exhibited nice electrocatalytic performance, although gradually degraded due to the Pt catalyst poisoning [14,15] (similar result to the electrode upon visible light irradiation by using >420 nm filter. Fig. S5). When the electrode was under visible light irradiation, the initial and steady–state of oxidation current density of electrode was further enhanced. Fig. 7B shows the peak current of MOR in the forward scan *vs* the cycle number of the CV scan on Pt/g-C_3N_4 electrode. The oxidation peak current density of Pt/g-C_3N_4 electrode decreased gradually with longer cycle numbers. The oxidation peak current density decreased *ca.* 35.6% after 300 cycles compared to the maximum value of 193.3 mA mg^{-1}. However, when the Pt/g-C_3N_4 electrode was under visible light illumination, the oxidation peak current densities displayed higher and more stable, which the peak current density only decreased *ca.* 8.8% after 300 cycles compared to the maximum value of 520.4 mA mg^{-1}. This finding indicates that the Pt/g-C_3N_4 electrode has more durable and higher catalytic performance for MOR, which is also consistent with the above CVs and EIS measurements.

4. Conclusions

In conclusion, ultrathin 2D g-C_3N_4 could be worked as efficient support for the deposition of ultrasmall Pt nanoclusters. The average size of Pt nanoclusters is about 3.2 nm. The as-prepared Pt/g-C_3N_4 nanosheets modified electrode exhibited enhanced electrocatalytic ability in MOR compared to bare Pt nanoparticles. More interestingly, when this electrode was upon visible light irradiation, higher and more stable performance of MOR were clearly observed compared with traditional ambient electrocatalytic oxidation. The synergistic effects of electro- and photo- catalytic MOR together with efficient interfacial electron transfer of the Pt/g-C_3N_4 contribute to the improved catalytic performance. This result shows that the 2D ultrathin g-C_3N_4 nanosheets can be used as promising photoactived support in the fields of solar and chemical energy conversion and also provides more insights into developing novel visible light photoactived electrode in direct methanol fuel cell.

Acknowledgments

This work was sponsored by K.C. Wang Magna Fund in Ningbo University. We also appreciate NSFC (21603111, 51373111) and Suzhou Nano-project (ZXG2012022).

Appendix A. Supplementary data

Supplementary data associated with this article can be found, in the online version, at http://dx.doi.org/10.1016/j.apcatb.2016.10.012.

References

[1] H.J. Lewerenz, C. Heine, K. Skorupska, N. Szabo, T. Hannappel, T. Vo-Dinh, A. Campbell, H.W. Klemm, A.G. Munoz, Energy Environ. Sci. 3 (2010) 748–760.
[2] C. Ampelli, G. Centi, R. Passalacqua, S. Perathoner, Energy Environ. Sci. 3 (2010) 292–301.
[3] H.J. Zhang, G.H. Chen, D.W. Bahnemann, J. Mater. Chem. 19 (2009) 5089–5121.
[4] S. Sfaelou, P. Lianos, AIMS Mater. Sci. 3 (2016) 270–288.
[5] K. Drew, G. Girishkumar, K. Vinodgopal, P.V. Kamat, J. Phys. Chem. B 109 (2005) 11851–11857.
[6] C. Zhai, M. Zhu, D. Bin, H. Wang, Y. Du, C. Wang, P. Yang, ACS Appl. Mater. Interfaces 6 (2014) 17753–17761.
[7] N. Mojumder, S. Sarker, S.A. Abbas, Z. Tian, V. Subramanian, ACS Appl. Mater. Interfaces 6 (2014) 5585–5594.
[8] T. Wang, J. Tang, S.C. Wu, X.L. Fan, J.P. He, J. Power Sources 248 (2014) 510–516.
[9] C.Y. Su, Y.C. Hsueh, C.C. Kei, C.T. Lin, T.P. Perng, J. Phys. Chem. C 117 (2013) 11610–11618.
[10] C. Wang, R. Yue, H. Wang, C. Zou, J. Du, F. Jiang, Y. Du, P. Yang, C. Wang, Int. J. Hydrogen Energy 39 (2014) 5764–5771.
[11] X.L. Fan, C.X. Zhang, H.R. Xue, H. Guo, L. Song, J.P. He, RSC Adv. 5 (2015) 78880–78888.
[12] A. Leelavathi, G. Madras, N. Ravishankar, J. Am. Chem. Soc. 136 (2014) 14445–14455.
[13] C. Zhai, M. Zhu, F. Pang, D. Bin, C. Lu, M.C. Goh, P. Yang, Y. Du, ACS Appl. Mater. Interfaces 8 (2016) 5972–5980.
[14] M.G. Hosseini, M.M. Momeni, Electrochim. Acta 70 (2012) 1–9.
[15] Y.Y. Song, Z.D. Gao, P. Schmuki, Electrochem. Commun. 13 (2011) 290–293.
[16] M. Zhu, P. Chen, M. Liu, Langmuir 28 (2012) 3385–3390.
[17] Y.J. Zhang, T. Mori, J.H. Ye, Sci. Adv. Mater. 4 (2012) 282–291.
[18] X.C. Wang, S. Blechert, M. Antonietti, ACS Catal. 2 (2012) 1596–1606.
[19] X.H. Li, M. Antonietti, Chem. Soc. Rev. 42 (2013) 6593–6604.
[20] S.W. Cao, J.X. Low, J.G. Yu, M. Jaroniec, Adv. Mater. 27 (2015) 2150–2176.
[21] X.C. Wang, X.F. Chen, A. Thomas, X.Z. Fu, M. Antonietti, Adv. Mater. 21 (2009) 1609–1612.
[22] X.J. Bai, R.L. Zong, C.X. Li, D. Liu, Y.F. Liu, Y.F. Zhu, Appl. Catal. B: Environ. 147 (2014) 82–91.
[23] Y. Di, X.C. Wang, A. Thomas, M. Antonietti, ChemCatChem 2 (2010) 834–838.
[24] Z.X. Ding, X.F. Chen, M. Antonietti, X.C. Wang, ChemSusChem 4 (2011) 274–281.
[25] X.G. Li, W.T. Bi, L. Zhang, S. Tao, W.S. Chu, Q. Zhang, Y. Luo, C.Z. Wu, Y. Xie, Adv. Mater. 28 (2016) 2427–2431.

[26] C. Lu, P. Zhang, S. Jiang, X. Wu, S. Song, M. Zhu, Z. Lou, Z. Li, F. Liu, Y. Liu, Y. Wang, Z. Le, Appl. Catal. B: Environ. 200 (2017) 378–385.
[27] M. Zhu, Y. Dong, Y. Du, Z. Mou, J. Liu, P. Yang, X. Wang, Chem. Eur. J. 18 (2012) 4367–4374.
[28] X.H. Li, J.M. Zhu, B.Q. Wei, Chem. Soc. Rev. 45 (2016) 3145–3187.
[29] M. Zhu, P. Chen, M. Liu, ACS Nano 5 (2011) 4529–4536.
[30] Q.J. Xiang, J.G. Yu, M. Jaroniec, J. Phys. Chem. C 115 (2011) 7355–7363.
[31] S.M. Fang, X.D. Dong, Y.C. Zhang, M.M. Kang, S.L. Liu, F.F. Yan, L.H. He, X.Z. Feng, P.Y. Wang, Z.H. Zhang, New J. Chem. 38 (2014) 5935–5942.
[32] K. Zhang, F. Ren, H. Wang, C. Wang, M. Zhu, Y. Du, ChemPlusChem 80 (2015) 529–535.
[33] K. Koczkur, Q. Yi, A. Chen, Adv. Mater. 19 (2007) 2648–2652.
[34] M. Umeda, M. Kokubo, M. Mohamedi, I. Uchida, Electrochim. Acta 48 (2003) 1367–1374.
[35] R. Yue, Q. Zhang, C. Wang, Y. Du, P. Yang, J.K. Xu, Electrochim. Acta 107 (2013) 292–300.
[36] C. Wang, H. Wang, C. Zhai, F. Ren, M. Zhu, P. Yang, Y. Du, J. Mater. Chem. A 3 (2015) 4389–4398.